Natural genetic variation screen in *Drosophila* identifies Wnt signaling, mitochondrial metabolism, and redox homeostasis genes as modifiers of apoptosis

Rebecca A.S. Palu*, Elaine Ong*, Kaitlyn Stevens*, Shani Chung*, Katie G. Owings*, Alan G. Goodman[†,‡], Clement Y. Chow*

*Department of Human Genetics, University of Utah School of Medicine, Salt Lake City, UT 84112

[†]School of Molecular Biosciences, Washington State University College of Veterinary Medicine, Pullman, WA 99164

[‡]Paul G. Allen School for Global Animal Health, Washington State University College of Veterinary Medicine, Pullman, WA 99164

Running title: Natural modifiers of apoptosis

Key words: apoptosis, *Drosophila*, genetic variation, modifier genes

Corresponding author:

Clement Y. Chow

15 N 2030 E

Rm 5200

Eccles Institute of Human Genetics

Salt Lake City, UT 84112

801-585-3314

cchow@genetics.utah.edu

ABSTRACT

Apoptosis is the primary cause of degeneration in a number of neuronal, muscular, and metabolic disorders. These diseases are subject to a great deal of phenotypic heterogeneity in patient populations, primarily due to differences in genetic variation between individuals. This creates a barrier to effective diagnosis and treatment. Understanding how genetic variation influences apoptosis could lead to the development of new therapeutics and better personalized treatment approaches. In this study, we examine the impact of the natural genetic variation in the *Drosophila* Genetic Reference Panel (DGRP) on two models of apoptosis-induced retinal degeneration: overexpression of *p53* or *reaper* (*rpr*). We identify a number of known apoptotic, neural, and developmental genes as candidate modifiers of degeneration. We also use Gene

Set Enrichment Analysis (GSEA) to identify pathways that harbor genetic variation that impact these apoptosis models, including Wnt signaling, mitochondrial metabolism, and redox homeostasis. Finally, we demonstrate that many of these candidates have a functional effect on apoptosis and degeneration. These studies provide a number of avenues for modifying genes and pathways of apoptosis-related disease.

INTRODUCTION

Phenotypic heterogeneity is the driving force behind the Precision Medicine Initiative (Scriver and Waters 1999; Nadeau 2001; Queitsch *et al.* 2012; Gallati 2014). Patients suffering from the same genetic disorders can carry identical causal mutations but often display wildly variable phenotypes and symptom severity. A large part of this variation is due to inter-individual differences in genetic background, including silent cryptic genetic variation that is revealed upon disease or stress (Queitsch *et al.* 2012; Chow 2016). Understanding the role of this variation and the genes or pathways which modify disease will lead to improved personalized therapeutic predictions, strategies, and diagnostics.

One process implicated in many genetic disorders is programmed cell death or apoptosis (Elmore 2007; Sano and Reed 2013; Kurtishi *et al.* 2018). During normal development and tissue turnover, cells can receive both internal and external signals that trigger a programmed response which eventually results in the death of the cell (Elmore 2007). Because cell death is essential to cellular, tissue, and organismal homeostasis, disruption of apoptosis pathways can be catastrophic. Inhibition of

apoptosis is an important step in transformation and cancer, while excess apoptosis, often activated by chronic cellular stress, is a primary cause of degeneration in different neuronal, retinal, muscular-skeletal, and metabolic diseases (Mattson 2000; Elmore 2007; Ouyang *et al.* 2012). As a result, an important area of therapeutic development is focused on targeting apoptosis without disrupting normal tissue homeostasis (Elmore 2007). Our previous work demonstrated that variation in apoptotic genes is associated with phenotypic variation in a model of retinal degeneration, suggesting that modifiers of apoptosis could serve as drug targets in degenerative diseases (Chow *et al.* 2016).

Model organism tools, such as the *Drosophila* Genetic Reference Panel (DGRP), enable the study of the impact of natural genetic variation on diseases and related pathways. The DGRP is a collection of ~200 isogenic strains derived from a wild population, such that each strain represents one wild-derived genome (Mackay *et al.* 2012). The variation in the DGRP is well tolerated under healthy, non-disease conditions and allows for the identification of genetic polymorphisms that are associated with phenotypic variation in models of human disease (Chow and Reiter 2017). Importantly, the availability of full-genome sequence for these strains allows for genome-wide association analyses that link quantitative phenotypes with genetic variation and modifier genes.

In this study, we report the results of natural variation screens of *reaper*- (*rpr*) and *p53*-induced apoptosis (Figure 1). Overexpression of either of these genes leads to massive apoptotic activation (Hay *et al.* 1995; Jin *et al.* 2000). While there is a great deal of

overlap between these pathways, they can each activate apoptosis independently. p53 is stabilized in response to DNA damage and initiates apoptosis by transcriptionally activating the inhibitor of apoptosis (IAP) inhibitors *rpr*, *grim*, and *hid* (Mollereau and Ma 2014) (Figure 1). It also induces the expression of the *Drosophila* TNF *eiger*, which subsequently increases apoptosis by activating JNK signaling and stabilizing the IAP inhibitor Hid (Shklover *et al.* 2015). *rpr* is activated transcriptionally by either p53 or the JNK signaling cascade, which is induced downstream of oxidative, ER, and other cellular stresses (Kanda and Miura 2004; Shlevkov and Morata 2012) (Figure 1). We designed this study to identify genetic modifiers of general apoptosis as well as modifiers that are specific to stress-induced, p53-independent pathways.

We observed substantial phenotypic variation across the DGRP for both *rpr*- and *p53*-induced apoptosis. Using genome-wide association analysis, we identified a number of modifying pathways and genes, several of which have known roles in cell death pathways, neuronal development, neuromuscular diseases, and cancer. Using systems biology approaches, we also identified Wnt signaling, mitochondrial redox homeostasis, and protein ubiquitination/degradation as possible modifiers of apoptosis. Finally, we confirmed that loss of many of these candidate modifier genes significantly alters degeneration. Our findings highlight several exciting new areas of study for apoptotic modifiers, as well as a role for stress-induced cell death in the regulation of degenerative disorders.

METHODS

116 **Fly stocks and maintenance**

117 Flies were raised at room temperature on a diet based on the Bloomington Stock Center
118 standard medium with malt. The strains containing *GMR-GAL4* and *UAS-p53* or *GMR-*
119 *rpr* on the second chromosome (*GMR>p53* and *GMR-rpr*) have been previously
120 described (Hay *et al.* 1995; Jin *et al.* 2000). These are referred to as the apoptotic
121 models throughout the manuscript. 204 strains from the DGRP were used for the
122 *GMR>p53* study (Table S1) and 202 were used for the *GMR-rpr* study (Table S2). In
123 both cases virgin females carrying one of the apoptosis models were crossed to males
124 of the DGRP strains. F1 progeny carrying *GMR>p53* or *GMR-rpr* were collected and
125 scored for eye size. The following RNAi and control strains are from the Bloomington
126 Stock Center: *swim* RNAi (55961), *CG3032* RNAi (57560), *LysRS* RNAi (32967),
127 *αMan1a* RNAi (64944), *LIMK1* RNAi (62153), *hay* RNAi (53345), *CG1907* RNAi
128 (38998), *Sema1a* RNAi (34320), *MED16* RNAi (34012), *bru1* RNAi (44483), *CycE* RNAi
129 (33645), *shab* RNAi (55682), *CG31559* RNAi (64671), *Cyt-c-P* RNAi (64898), *Ir40A*
130 (57566), *sif* RNAi (61934), control *attP40* (36304), and control *attP2* (36303).
131
132 **Eye size imaging**
133 For eye images, adult females were collected under CO_2 anesthesia and aged to 2-7
134 days, then flash frozen on dry ice. Left eyes were imaged for all measurements. 10-15
135 eyes per strain were imaged at 3X magnification using a Leica EC3 camera. Eye area
136 was measured in ImageJ as previously described (Chow *et al.* 2016).
137
138 **Phenotypic analysis and genome-wide association**

For each DGRP line, eyes from 10-15 individual females were imaged and measured. The P-values for association of genetic background and eye size for each model were calculated using one-way ANOVA on R software. Mean eye area was used for the genome-wide association (GWA). GWA was performed as previously described (Chow *et al.* 2016). DGRP genotypes were downloaded from the website, http://dgrp.gnets.ncsu.edu/. Variants were filtered for minor allele frequency (≥ 0.05), and non-biallelic sites were removed. A total of 1,967,719 variants for *p53* and 1,962,205 variants for *rpr* were included in the analysis. Mean eye size for 2953 F1 DGRP/*GMR>p53* or 2987 DGRP/*GMR-rpr* F1 progeny were regressed on each SNP. To account for cryptic relatedness (He *et al.* 2014; Huang *et al.* 2014), GEMMA (v. 0.94) (Zhou and Stephens 2012) was used to both estimate a centered genetic relatedness matrix and perform association tests using the following linear mixed model (LMM):

$$y=\alpha+x\beta+u+\square$$

$$u \sim MVN_n (0,\lambda\tau^{-1} K)$$

$$\square \sim MVN_n (0,\tau^{-1} I_n)$$

where, as described and adapted from Zhou and Stephens 2012, y is the n-vector of mean eye sizes for the n lines, α is the intercept, x is the n-vector of marker genotypes, β is the effect size of the marker. u is a n x n matrix of random effects with a multivariate normal distribution (MVN_n) that depends on λ, the ratio between the two variance components, τ^(-1), the variance of residuals errors, and where the covariance matrix is informed by K, the calculated n x n marker-based relatedness matrix. K accounts for all pairwise non-random sharing of genetic material among lines. □, is a n-vector of residual errors, with a multivariate normal distribution that depends on τ^(-1) and I_n,

the identity matrix. Genes were identified from SNP coordinates using the BDGP R54/dm3 genome build. A SNP was assigned to a gene if it was +/- 1 kb from a gene body.

Correlation Analysis

Correlation analyses were performed to compare mean eye size in DGRP strains between *GMR>p53*, *GMR-rpr*, and *GMR>Rh1*^{G69D} (Chow *et al.* 2016). Statistics were calculated using a Pearson Correlation Test using R software.

RNAi Validation

Virgin females from the apoptotic models were crossed to males carrying RNAi constructs targeting candidate modifiers of those models, and the eye size of F1 progeny expressing both the apoptotic model and the RNAi construct was measured as described above. The eyes of 10-15 females were imaged and measured. Eye size from RNAi-carrying strains were compared directly to genetically matched *attP40* or *attP2* controls using a Dunnett's multiple comparisons test.

Bioinformatics Analysis

Genetic polymorphisms were associated with candidate genes within 1 kb of the polymorphism. Information about candidate genes and their human orthologues was gathered from a number of databases including Flymine, Flybase, OMIM, and NCBI. Genetic interaction maps were generated using the GeneMANIA plugin on Cytoscape (version 3.6.1) (Shannon *et al.* 2003; Montojo *et al.* 2010). GSEA was run to generate a

185 rank-list of genes based on their enrichment for significantly associated polymorphisms.
186 For GSEA analysis, polymorphisms within 1kb of more than 1 gene were assigned to
187 one gene based on a priority list of exon, UTR, intron, and upstream or downstream.
188 Genes were assigned to GO categories, and calculation of enrichment score was
189 performed as described (Subramanian *et al.* 2005). Categories with ES scores > 0
190 (enriched for associated genes with low p-values), gene number > 3, and p-values
191 <0.05 were included in the final output.
192

193 ## RESULTS AND DISCUSSION

194 ### *rpr*- and *p53*-induced apoptosis is dependent on genetic background

195 We used the *Drosophila* eye to model apoptosis. Expression of either *p53* or *rpr* in the
196 ommatidial array of the developing eye imaginal disc results in massive cell death and
197 smaller, rough adult eyes (Hay *et al.* 1995; Jin *et al.* 2000). The *rpr* model is induced by
198 direct drive of the *GMR* promoter (*GMR-rpr*) on a second chromosome balancer. The
199 *p53* model is induced using the *GAL4/UAS* system, where *GMR-GAL4* drives
200 expression of *UAS-p53* (*GMR>p53*). Importantly, in both of these models, adult eye size
201 is an easily scorable, quantitative proxy for levels of apoptosis. The lines described
202 serve as the donor strains (*GMR>p53/CyO* or *GMR-rpr,CyO/sna*^{sco}) that we crossed to
203 each DGRP strain. Females from the donor strains were crossed with males of each of
204 204 or 202 DGRP strains to generate F1 progeny that overexpressed *p53* or *rpr*,
205 respectively, in the eye disc. The progeny received 50% of their genome from the
206 maternal donor strain and 50% from the paternal DGRP strain. Therefore, we are
207 measuring the dominant effect of the DGRP background on the *p53* or *rpr* retinal

208 phenotype. This cross design is similar to a study of ER stress-induced degeneration
209 (Chow *et al.* 2016) and a model of Parkinson's Disease (Lavoy *et al.* 2018) we
210 previously reported. We examined eye size in the F1 progeny to determine the average
211 eye size in individual genetic backgrounds (Figure 2A-D).
212
213 We first tested the effect of sex on apoptosis in a pilot study. We measured eye area in
214 at least ten females and ten males from eight different DGRP strains crossed to either
215 the *p53* or *rpr* model. Eye size is positively correlated between males and females
216 (Figure S1A,B). Because variation is greater in females (Figure S1A,B), we elected to
217 focus on female eye size for the remainder of our analysis.
218
219 We found a significant effect of genetic background on eye size in the *GMR>p53* model
220 ($P < 2.2 \times 10^{-16}$) (Figure 2A,C, Table S1). Average eye size measured in pixels on
221 ImageJ ranged from 10542 pixels (RAL812) to 17835 pixels (RAL374) (Table S1).
222 Similarly, we found a significant effect of genetic background on eye size in the *GMR-*
223 *rpr* model ($P < 2.2 \times 10^{-16}$), with median eye size ranging from 7957 pixels (RAL83) to
224 16884 pixels (RAL304) (Figure 2B,D, Table S2). For both the *GMR>p53* and the *GMR-*
225 *rpr* models, the variation in eye size within individual DGRP strains is substantially
226 smaller than the variation observed between DGRP strains expressing the *GMR-rpr*
227 model (Figure 2A-B, Table S1-S2).
228
229 We noted that the range in average eye size for the *GMR-rpr* model (8927 pixels) is
230 greater than that seen in the *GMR>p53* model (7293 pixels). This could be due to the

231 greater involvement of *rpr* in a variety of stress-induced, *p53*-independent apoptotic
232 pathways (Shlevkov and Morata 2012). Alternatively, it is possible that variation in *p53*-
233 associated pathways is simply less well-tolerated than in *rpr*-associated pathways. It is
234 also possible that the DGRP simply carries more variation affecting the *GMR-rpr* model
235 than *GMR>p53* model.
236
237 We observed qualitative differences between the apoptotic models, with flies expressing
238 the *GMR>p53* model displaying a teardrop-shaped eye (Figure 2C) and flies expressing
239 the *GMR-rpr* model displaying a rounder eye (Figure 2D). These qualitative shapes
240 were not subject to effects of genetic variation. The differences in eye shape noted
241 between *GMR>p53* and *GMR-rpr*, however, could be indicative of differences in the
242 mechanisms by which apoptosis and degeneration progress in these two models.
243 Alternatively, this could be evidence of the technical differences in the two models,
244 since *p53* is driven by the *GAL4/UAS* system and *rpr* is driven directly by the *GMR*
245 promotor. We saw no accumulation of necrotic tissue in strains experiencing severe
246 degeneration, nor did we note obvious differences in pigmentation (Figure 2C,D). Eyes
247 from all strains maintained the rough-eye phenotype that is characteristic of *p53* or *rpr*-
248 induced degeneration, indicating that while modifying variation may reduce the amount
249 of cell death in the eye imaginal disc, it cannot fully rescue the degenerative phenotype.
250
251 **Apoptosis models correlate depending upon the pathway they activate**
252 Because canonical p53 signaling activates the expression of *rpr*, we expected high
253 correlation in apoptosis levels and eye size between these models (Shlevkov and

Morata 2012; Mollereau and Ma 2014). Indeed, there is a significant positive correlation in eye size between DGRP strains expressing *GMR>p53* and *GMR-rpr* (r = 0.19, p = 0.0071) (Figure 3A). In a previous study, we examined the impact of genetic variation on a model of retinitis pigmentosa (RP) and ER stress-induced apoptosis (Chow *et al.* 2016). In this study, we found that the degeneration induced by overexpression of a misfolded protein ($Rh1^{G69D}$) in the developing eye imaginal disc is modified by a number of genes involved in apoptosis (Chow *et al.* 2016). This is to be expected, as the primary cause of degeneration in this model is JNK-*hid/grim/rpr*-mediated cell death (Figure 1) (Kang *et al.* 2012). Consistent with this mechanism of $Rh1^{G69D}$-induced degeneration, we found a significant correlation in eye size between the $Rh1^{G69D}$ and *rpr* models (r = 0.25, p = 0.001, Figure 3B). In contrast, we see no correlation between the $Rh1^{G69D}$ and *p53* models of apoptosis (r = 0.12, p = 0.13) (Figure 3C). These results suggest that there is shared genetic architecture between $Rh1^{G69D}$ and *rpr*-mediated apoptosis and degeneration that is independent from that shared between *p53* and *rpr*.

rpr-induced degeneration is modified by apoptosis, Wnt signaling, and mitochondrial metabolism

Genome-wide association analysis: To identify the genes driving this phenotypic variability, we performed a genome-wide association analysis to identify genetic polymorphisms that impact the severity of degeneration in the *GMR>p53* and *GMR-rpr* models of apoptosis. We used mean eye size as a quantitative phenotype to test for association with polymorphisms in the DGRP. Using a p-value cutoff of $<1x10^{-04}$, we identified 128 significantly associated polymorphisms for the *GMR-rpr* model (Table S3).

We only considered polymorphisms that fall within +/- 1 kb of a gene. Sixteen polymorphisms lie outside of these parameters and were not considered further. Of the remaining 112 polymorphisms, ten are located in an intergenic region (+/- 1kb), 14 are located in UTRs, 69 are located in introns, and 19 are located in protein-coding sequences. All 19 polymorphisms in coding regions are synonymous variants. These 112 gene-associated polymorphisms lie in 82 candidate genes (Table S3, S4). Sixty-six of the candidate genes have direct human orthologues (Table S4). A more stringent p-value cutoff ($<1x10^{-5}$) yields only 20 polymorphisms, 16 of which lie in 14 candidate genes (12 with human orthologs) (Table S3, S4). Because the more stringent cutoff yielded few candidates, we focused the majority of our analysis on the 82 candidate genes identified at $p < 1x10^{-04}$.

For the *GMR>p53* model, we identified 24 polymorphisms at a p-value cutoff of $<1x10^{-04}$ (Table S5). Eight of these polymorphisms lie outside of genes and were not considered further. Of the remaining 16 polymorphisms, one is located in a UTR, 15 are located in introns, and eight are intergenic. The 16 gene-associated polymorphisms lie in 13 candidate genes (Table S5, S6). Thirteen of the associated polymorphisms have a p-value of $<1x10^{-05}$. Five of these are intergenic, while the remaining six are in six candidate genes. Interestingly, there is no overlap between the *GMR>p53* candidate polymorphisms or genes and those identified using the *GMR-rpr* model of apoptosis (Table S3-S6). The only overlap in modifier genes is between *GMR>Rh1*^{G69D} and *GMR>p53* (Table S6) (Chow *et al.* 2016). They share candidate modifier genes *CG31559*, a disulfide oxidoreductase (FlyBase Curators *et al.* 2004), and *dpr6,* a cell

surface immunoglobulin involved in synapse organization (Gaudet *et al.* 2011). It is unclear what the significance of this overlap might be.

We conclude from our initial analysis that the top candidates for our models of degeneration are highly specific to the method by which we induce that degeneration. Because there are so few significant associations for the *GMR>p53* model of apoptosis, and even fewer that are in close proximity to a candidate gene, we elected to focus the remaining analysis on the *GMR-rpr* model.

Modifier genes: Because the *rpr* model directly induces apoptosis, we expected to see apoptotic functions for many of the candidate genes identified in our GWAS. The top hit was the gene *echinus* (*ec*), a ubiquitin specific protease (USP) orthologous to human *USP53* and *USP54* (Table S4). We identified nine intronic SNPs in *ec* through our association analysis. Previous studies show that loss of *ec* in the developing eye results in a mild rough eye phenotype, albeit a much less dramatic one than that seen upon overexpression of *rpr* (Wolff and Ready 1991; Copeland *et al.* 2007). While this previous study reported no genetic interaction between *ec* and *rpr*, this was assessed based on qualitative changes as opposed to quantitative differences in eye size (Copeland *et al.* 2007). Our GWAS data suggests that such a genetic interaction may play an important role in *rpr*-induced degeneration.

Ec is one of several apoptotic genes identified in this analysis. In fact, 16/82 (~20%) of the candidate genes have known functions in apoptosis-related pathways, all of which

have conserved human orthologues (Table S4). One of these is *Diap2*, a *Drosophila* paralog of *Diap1* (human orthologs: *BIRC2* and *BIRC3*) (Hay *et al.* 1995). The Diap proteins normally inhibit caspase activation and prevent apoptosis. Expression of the rpr/grim/hid proteins inhibits Diap1 and Diap2, allowing apoptosis to proceed. Increased expression or activity of Diap2 reduces the impact of *rpr* overexpression, thereby reducing apoptosis (Hay *et al.* 1995). Conversely, reduced expression of *Diap2* may not have a strong impact on *rpr*-associated degeneration, as *Diap1* is the major functional paralog in this pathway. The identification of a gene directly involved in the *rpr* pathway demonstrates the efficacy of our GWAS.

Two candidates, *hay* and *Xpd* (*ERCC3* and *ERCC2*) (Table S4), have human orthologs mutated in Xeroderma pigmentosum, an inherited genetic condition where defects in DNA excision repair result in melanomas and eventually death (Kraemer and DiGiovanna 2016). These are subunits of the TFIIH helicase complex that are involved in excision repair after UV damage (Koken *et al.* 1992; Mounkes *et al.* 1992; Reynaud *et al.* 1999). Besides *hay* and *Xpd*, we identified 4 additional genes whose human orthologs are directly involved in cancer: *DIP-iota* (*OPCML*), *Fum4* (*FH*), *CG8405* (*TMEM259*), and *CG15529* (*BLNK*). Mutations in these genes have been associated with ovarian cancer (*OPCML*) (Sellar *et al.* 2003), renal cancer (*FH*) (The Multiple Leiomyoma Consortium 2002; Pollard *et al.* 2005), and various carcinomas (*TMEM259*) (Chen *et al.* 2005). The roles of these genes in cancer are likely due to functions in apoptotic initiation or cell cycle regulation. Other candidates are activated downstream of p53, such as *CG44153* (*ADGRB3*) and *stac* (*BAIAP3*) (Shiratsuchi *et al.* 1997, 1998).

This suggests that feedback signaling through p53 can increase *rpr*-induced apoptosis and degeneration.

24/82 candidate genes (~30%) are involved in neuronal function or implicated in neurological disease. Twenty-three have conserved human orthologues (Table S4). Human orthologs of *Form3* (*INF2*) and *LysRS* (*KARS*) can both be mutated in different forms of the degenerative peripheral neuropathy Charcot-Marie-Tooth disease (McLaughlin *et al.* 2010; Boyer *et al.* 2011), while *Shawl* (*KCNC3*) and *CG7741* (*CWF19L1*) are associated with spinocerebellar ataxia (Waters *et al.* 2006; Burns *et al.* 2014). Mutation in the Rab3-interacting scaffold protein encoded by *Rim* (*RIMS1*) can cause a retinal degenerative disease that is similar to retinitis pigmentosa (Johnson *et al.* 2003), which was the focus of the $Rh1^{G69D}$ study (Chow *et al.* 2016). Identification of genes with roles in different neuronal and muscular degenerative diseases suggests that these modifiers could be important in a variety of apoptosis-associated diseases.

Network analysis: To understand if there are functional relationships between *GMR-rpr* modifiers, we examined interactions among the 82 candidate genes. Genetic, physical, and predicted interactions were compiled and visualized using Cytoscape software (Shannon *et al.* 2003; Montojo *et al.* 2010). Fourteen of the 82 candidate genes were found as nodes in these interaction networks, as was *rpr* itself (Figure 4A). We identified several interesting clusters of candidate genes, including those with functions in apoptosis, development, and protein ubiquitination.

As expected, given the large number of candidates with apoptotic roles, we found an apoptosis cluster of interactions between modifiers with functions associated with cell cycle regulation and cell death (Figure 4A). A number of these genes, including *Diap2* and *cher* (*FLNA*), have either direct or indirect interactions with *rpr* itself. As noted above, *Diap2* interacts both physically and genetically with *rpr* (Figure 1) (Hay *et al.* 1995). *cher* shows indirect genetic interactions with *rpr* through its physical association with the presenillin (*psn*) protein (Guo *et al.* 2000) (Figure 4A). This interaction is conserved in humans and is specifically associated with Alzheimer's Disease (Lu *et al.* 2010).

We also observed a cluster composed of regulators of developmental apoptosis in our network, including the *ec* protease (Copeland *et al.* 2007) and the neuronal cell adhesion protein encoded by *kirre* (*KIRREL3*) (Bao *et al.* 2010) (Figure 4A). Indirect genetic interactions were identified between these genes, which are commonly involved in development of the *Drosophila* eye imaginal disc and accompanying regulated apoptosis. The chromatin-binding HmgD/Z (*HMGB2*) proteins are expressed at high levels in the larval CNS, suggesting that they are important for the developmental regulation of neuronal gene expression (Churchill *et al.* 1995; Gaudet *et al.* 2011; Brown *et al.* 2014). They indirectly interact with *rpr* through the closely related *dsp1,* which encodes another paralog of human *HMGB2* (Figure 4A). Dsp1 recruits members of the repressive polycomb complex to chromatin. It is possible that these genetic interactions indicate a role for the HMGB2 proteins in regulating *rpr* expression and, as a result, developmental regulation of cell death and tissue turnover. Our apoptotic model is

392 expressed in a developmental tissue, suggesting that some of the variation in eye size
393 observed across the DGRP could be due to changes in the response of developmental
394 processes to the abnormal activation of apoptosis. Such regulators of developmental
395 apoptosis could be excellent candidates for therapeutic targeting in degenerative
396 diseases.
397
398 We also identified a number of predicted interactions in a cluster of modifier genes
399 involved in protein ubiquitination (Figure 4A). Among the top candidate genes are *ec*,
400 *Diap2*, *Su(dx)* (*ITCH*), and *Roc2* (*RNF7*), all of which have important roles in protein
401 degradation through ubiquitination and the proteasome degradation pathway. *Su(dx)*,
402 like *Diap2*, encodes a ubiquitin ligase (Gaudet *et al.* 2011). Our network analysis
403 highlights a predicted interaction between *Su(dx)* and the Rab GTPase-interacting
404 protein *Evi5*, another candidate gene (Laflamme *et al.* 2012) (Figure 4A). This regulator
405 of vesicular fusion is predicted to interact with a number of additional ubiquitin ligases
406 as well (Figure 4A). Degradation of proteins through the proteasome is an important
407 mechanism for maintaining cellular homeostasis under a variety of cellular stresses
408 (Sano and Reed 2013). Altered regulation of E3 ligases, which determine the identity
409 and specificity of proteins for degradation (Ester Morreale and Walden 2016), could tip
410 the balance of cells experiencing apoptotic stress toward or away from cell death.
411
412 **Gene set enrichment analysis:** Thus far, we have focused our analysis on rank-order
413 candidate modifiers identified in our GWAS. While this provides many new avenues for
414 future analysis, it ignores the majority of the association data. We therefore performed

gene set enrichment analysis (GSEA), using all GWAS variant data and their associated P-values. The gene nearest to each variant was assigned the variant's P-value and used as GSEA input, using the method described (Subramanian *et al.* 2005). Given a defined set of genes annotated with a certain GO function, GSEA determines whether the members of that set are randomly distributed throughout the ranked list or if they are found primarily at the top or bottom of that list. GO categories enriched at the top of the list functionally describe the phenotype of the gene set. While traditional GO analysis uses a set of genes based on a P-value cutoff, GSEA examines the entire gene set (Dyer *et al.* 2008). GSEA identified 62 significantly associated gene sets (≥ 3 genes) at a p-value of <0.05 (Table S7). The top gene set was synaptogenesis (GO:0007416, P = 3.7×10^{-3}) and includes *Sema1a* (*SEMA6A*), a conserved semaphorin-binding protein involved in axon guidance (Ayoob *et al.* 2006; Gaudet *et al.* 2011) and one of the top modifier candidates based on individual polymorphism analysis (Figure 4B, Table S7). Other genes in this category include those involved in synapse formation and organization, suggesting that regulating neuronal connectivity and synapse choice could play a role in the decision to apoptose or to survive.

The second most significantly enriched category was Wnt signaling (GO:0016055, P = 6.7×10^{-3}), consisting of 51 enriched genes from our *GMR-rpr* analysis (Figure 4B, Table S7). One of these, *arr*, is also a candidate modifier gene (Table S4,S7). *arr* is a *Drosophila* orthologue of the genes encoding the co-receptors *LRP5/6* in canonical Wnt signaling (Rives *et al.* 2006). The second most significant single candidate gene in the GWA is *swim* (*TINAGL1*/*TINAG*), a secreted cysteine protease capable of binding the

438 wingless (wg) ligand and enhancing its spread and signaling capabilities (Mulligan *et al.*
439 2012). Also enriched for significant polymorphisms are four frizzled paralogs (Wnt
440 receptors) and six paralogs of the Wnt ligand (Table S7). Other integral components of
441 the canonical Wnt pathway, such as *disheveled*, *axin*, and *CKIα*, are enriched for
442 associated polymorphisms, as are several peripheral and non-canonical regulators of
443 Wnt signaling (Table S7). This striking association is reinforced by previous studies that
444 have linked Wnt signaling with either the promotion or restraint of cell death (Pećina-
445 Slaus 2010). Non-canonical Wnt signaling can activate JNK or calcium release from the
446 ER, both of which can alter the decision to initiate apoptosis (Rasmussen *et al.* 2018). It
447 will be interesting to investigate Wnt signaling collectively as well as with individual
448 candidates to determine how different branches of the pathway impact degenerative
449 diseases.
450
451 GSEA also identified a number of genes and pathways involved in mitochondrial
452 homeostasis and metabolism (Figure 4B), including malate metabolic processes (seven
453 genes, GO:0006108, P = 0.011). These genes encode for malate dehydrogenase
454 enzymes, six of which are localized to the mitochondrion (Figure 4B, Table S7). Malate
455 dehydrogenase catalyzes the oxidation of malate to oxaloacetate in the last step of the
456 TCA cycle prior to the entrance of acetyl-CoA (Minárik *et al.* 2002). The presence of so
457 many paralogs of this enzyme suggests that mitochondrial metabolism, and in particular
458 the mitochondrial redox state, is a major regulator of apoptosis. Supporting this, one of
459 the top candidates, Fum4 (*FH*), is also an essential enzyme in the TCA cycle (Table
460 S4). The GSEA further supports this finding, as FAD binding is also enriched (48 genes,

GO:0050660, P = 0.020) (Figure 4B). A primary function for these 48 enriched genes is the maintenance of redox homeostasis, 16 of which localize to the mitochondria. Another of these genes, the apoptosis-inducing factor *AIF*, is activated independently from caspases by mitochondrial stress and is released into the cytoplasm, travels to the nucleus, and initiates the chromatin condensation and DNA fragmentation that immediately precedes cell death (Elmore 2007).

More generally, redox homeostasis in other cellular compartments is also implicated by GSEA (Table S7, Figure 4B). Three paralogs of aldehyde oxidase (*Aox*) and the NAD(P)H oxidoreductase *Duox* (*DUOX1*) are enriched for associated polymorphisms; these oxidase enzymes are essential for maintaining an appropriate balance of reactive oxygen species in the cytoplasm. We identified four paralogs of acyl-coA oxidase (*Acox*), which is involved in the β-oxidation of very long chain fatty acids in the peroxisome, and an additional 4 genes involved in mitochondrial β-oxidation: *wal* (*ETFA*), *Mcad* (*ACADM*), *CG4860* (*ACADS*), and *CG7461* (*ACADVL*).

The involvement of enzymes regulating redox homeostasis, and more specifically redox homeostasis in the mitochondria, is consistent with *rpr*-induced apoptosis. Both caspase-dependent and caspase-independent apoptotic pathways can be activated downstream of mitochondrial stress (Elmore 2007; Rasmussen *et al.* 2018). Increasing the permeability of the mitochondrial membrane is sufficient to ensure activation of the apoptosome through the release of cytochrome-C (Elmore 2007). This, along with expression of the mitochondria-associated IAP inhibitors rpr/grim/hid, activates the

484 caspase cascade (Sandu *et al.* 2010). Damage to the mitochondria that increases
485 permeability, such as through redox stress, is itself sufficient to activate apoptosis in a
486 caspase-independent manner through the release of AIF (Elmore 2007).
487
488 Other metabolic processes such as sterol transport (GO:0015918, P = 0.013), leucine
489 import (GO:0060356, P = 8.9 x 10^{-3}), and fat body development (GO:0007503, P =
490 0.011) are enriched in the GSEA (Table S7, Figure 4B). Disruption of metabolic
491 processes has long been known to induce oxidative and ER stress, both of which are
492 capable of activating apoptosis through JNK/*grm-rpr-hid* signaling cascades or directly
493 through mitochondrial stress (Kanda and Miura 2004). It will be interesting to explore
494 how these metabolic processes alter apoptosis not only in this model of retinal
495 degeneration, but in physiologically relevant cell types and tissues, such as the midgut,
496 fat body, and insulin-producing cells.
497
498 The enrichment of multiple metabolic categories suggests that the impact of cellular and
499 mitochondrial metabolism on redox homeostasis could play a major role in *rpr*-induced
500 degeneration. We hypothesize that these regulators of mitochondrial redox state and
501 metabolism are directly and indirectly influencing the activation of mitochondrial proteins
502 involved in the final decision to undergo apoptosis. Our GSEA emphasizes the
503 importance of exploring not just individually associated genes but also their functional
504 pathways and partners when identifying genetic modifiers of disease.
505
506 **Functional analysis of candidate modifiers of apoptosis**

To confirm the roles of our candidate genes in regulating apoptosis, we elected to test the impact of loss of modifier expression for nine of the most significant rank-ordered candidate genes. We crossed RNAi targeting each of these modifiers into the *GMR-rpr* or *GMR>p53* line, and then measured the eye area in offspring carrying both the RNAi construct and the apoptosis model (Figure 5, Figure S2). Eye area was quantified and compared to a genetically matched control expressing only the apoptosis model (Figure S3A). Due to a lack of highly significant candidate modifiers of *p53*-induced apoptosis, we focus our analysis here on the *rpr* modifiers. Knockdown of either *LIMK1* (*LIMK1*) (16183 ± 875 pixels, N = 15) or *swim* expression (15518 ± 2418 pixels, N = 14) resulted in enhancement of the apoptosis phenotype, showing a significant decrease in eye size compared to controls expressing only *GMR-rpr* (17534 ± 1098 pixels, N = 11) (Figure 5). Knockdown of *sema1a* (18990 ± 746 pixels, N = 15), *MED16* (*MED16*) (20323 ± 622 pixels, N = 15), or *hay* (20240 ± 617 pixels, N = 14) resulted in a partial rescue, with a significant increase in eye size compared to controls expressing *GMR-rpr* (Figure 5). No significant change in eye size was observed upon knockdown of *CG3032* (*GZF1*) (18525 ± 449 pixels, N = 12), *LysRS* (*KARS*) (17879 ± 1834 pixels, N = 12), *αMan-1A* (*MAN1A2*) (17842 ± 763 pixels, N = 15), or *CG1907* (*SLC25A11*) (18755 ± 787 pixels, N = 13) (Figure 5). No phenotype was observed for knockdown of any of the modifiers under non-apoptosis conditions (Figure S3B,C). These results demonstrate that many of the top GWA candidate modifiers are capable of modifying the apoptotic phenotypes associated with the *GMR-rpr* model of degeneration. In the future we will also examine the impact of overexpression of candidate genes on the GMR-rpr model of apoptosis,

529 as some candidate genes may exert a stronger influence under conditions of gain rather
530 than loss of function.
531
532 **CONCLUSIONS**
533 The primary goal of this study was to identify candidate genes and pathways that modify
534 apoptosis and degenerative processes. Apoptosis is a primary cause of disease in a
535 multitude of degenerative disorders (Mattson 2000). It is also a commonly targeted
536 pathway for cancer therapies (Ouyang *et al.* 2012). These and other diseases are
537 subject to a large degree of phenotypic heterogeneity due to inter-individual differences
538 in genetic background among patients (Queitsch *et al.* 2012; Chow 2016).
539 Understanding how genetic diversity in the population impacts apoptosis could therefore
540 lead to identification of prognostic predictors in the diagnosis of disease and of new
541 therapeutic targets. The modifiers identified here inform our understanding of cell death
542 regulation and could serve as therapeutic targets in a variety of apoptosis-related
543 disorders.
544
545 This study demonstrates the use of the DGRP to identify modifiers that are extremely
546 specific to the disease model being tested. Even though the end point of degeneration
547 is superficially the same for *rpr* and *p53* models, candidate modifier genes are unique to
548 each model. Our methods clearly identify genetic variation associated with specific
549 disease mechanisms, and not simply genes involved in general cell health and survival.
550 We believe the modifying genes and pathways discovered and discussed here are
551 excellent candidates in the treatment and understanding of apoptosis-related disorders.

With further analysis, we can characterize the roles these modifiers play in degeneration and their specific functions across tissues and disease models. The genes and pathways identified study have tremendous value as possible therapeutic targets or prognostic markers of disease.

ACKNOWLEDGEMENTS

We thank Andre Cruz and Demi Perez for their contributions to this project. This research was supported by an NIH/NIGMS R35 award (1R35GM124780) and a Glenn Award from the Glenn Foundation for Medical Research to CYC. CYC is the Mario R. Capecchi Endowed Chair in Genetics. RASP is supported by a NIDDK T32 fellowship (5T32DK110966). KGO is supported by the Genetics T32 Fellowship from the University of Utah. EO and KS were supported by the Undergraduate Research Opportunities Program (UROP) through the University of Utah Office of Undergraduate Research. AGG is supported by an NIH/NIAID R21 award (R21AI128103).

REFERENCES

Ayoob J. C., J. R. Terman, and A. L. Kolodkin, 2006 Drosophila Plexin B is a Sema-2a receptor required for axon guidance. Development 133: 2125–35. https://doi.org/10.1242/dev.02380

Bao S., K.-F. Fischbach, V. Corbin, and R. L. Cagan, 2010 Preferential adhesion maintains separation of ommatidia in the Drosophila eye. Dev. Biol. 344: 948–956. https://doi.org/10.1016/J.YDBIO.2010.06.013

Boyer O., F. Nevo, E. Plaisier, B. Funalot, O. Gribouval, *et al.*, 2011 *INF2* Mutations in Charcot–Marie–Tooth Disease with Glomerulopathy. N. Engl. J. Med. 365: 2377–2388. https://doi.org/10.1056/NEJMoa1109122

Brown J. B., N. Boley, R. Eisman, G. E. May, M. H. Stoiber, *et al.*, 2014 Diversity and dynamics of the Drosophila transcriptome. Nature 512: 393–399. https://doi.org/10.1038/nature12962

Burns R., K. Majczenko, J. Xu, W. Peng, Z. Yapici, *et al.*, 2014 Homozygous splice mutation in CWF19L1 in a Turkish family with recessive ataxia syndrome. Neurology 83: 2175–82. https://doi.org/10.1212/WNL.0000000000001053

Chen Y.-C., B. Davidson, C.-C. Cheng, A. Maitra, R. L. Giuntoli, *et al.*, 2005 Identification and characterization of membralin, a novel tumor-associated gene, in ovarian carcinoma. Biochim. Biophys. Acta - Gene Struct. Expr. 1730: 96–102. https://doi.org/10.1016/J.BBAEXP.2005.06.008

Chow C. Y., 2016 Bringing genetic background into focus. Nat. Rev. Genet. 17: 63–64. https://doi.org/10.1038/nrg.2015.9

Chow C. Y., K. J. P. Kelsey, M. F. Wolfner, and A. G. Clark, 2016 Candidate genetic modifiers of retinitis pigmentosa identified by exploiting natural variation in Drosophila. Hum. Mol. Genet. 25: 651–659. https://doi.org/10.1093/HMG/DDV502

Chow C. Y., and L. T. Reiter, 2017 Etiology of Human Genetic Disease on the Fly. Trends Genet. 33: 391–398. https://doi.org/10.1016/j.tig.2017.03.007

Churchill M. E., D. N. Jones, T. Glaser, H. Hefner, M. A. Searles, *et al.*, 1995 HMG-D is an architecture-specific protein that preferentially binds to DNA containing the dinucleotide TG. EMBO J. 14: 1264–75.

Copeland J. M., I. Bosdet, J. D. Freeman, M. Guo, S. M. Gorski, *et al.*, 2007 echinus, required for interommatidial cell sorting and cell death in the Drosophila pupal retina, encodes a protein with homology to ubiquitin-specific proteases. BMC Dev. Biol. 7: 1–15. https://doi.org/10.1186/1471-213X-7-82

Dyer M. D., T. M. Murali, and B. W. Sobral, 2008 The Landscape of Human Proteins Interacting with Viruses and Other Pathogens. PLoS Pathog. 4: e32. https://doi.org/10.1371/journal.ppat.0040032

Elmore S., 2007 Apoptosis: a review of programmed cell death. Toxicol. Pathol. 35: 495–516. https://doi.org/10.1080/01926230701320337

Ester Morreale F., and H. Walden, 2016 Types of Ubiquitin Ligases. https://doi.org/10.1016/j.cell.2016.03.003

FlyBase Curators, Swiss-Prot Project Members, and InterPro Project Members, 2004 Gene Ontology annotation in FlyBase through association of InterPro records with GO terms.

Gallati S., 2014 Disease-modifying genes and monogenic disorders: experience in cystic fibrosis. Appl Clin Genet 7: 133–146. https://doi.org/10.2147/TACG.S18675

Gaudet P., M. Livstone, and P. Thomas, 2011 Gene Ontology annotation inferences using phylogenetic trees. GO Reference Genome Project. Brief. Bioinform. 12: 449–462.

Guo Y., S. X. Zhang, N. Sokol, L. Cooley, and G. L. Boulianne, 2000 Physical and genetic interaction of filamin with presenilin in Drosophila. J. Cell Sci. 113.

Hay B. A., D. A. Wassarman, and G. M. Rubin, 1995 Drosophila homologs of baculovirus inhibitor of apoptosis proteins function to block cell death. Cell 83: 1253–1262. https://doi.org/10.1016/0092-8674(95)90150-7

He B. Z., M. Z. Ludwig, D. A. Dickerson, L. Barse, B. Arun, *et al.*, 2014 Effect of Genetic Variation in a *Drosophila* Model of Diabetes-Associated Misfolded Human Proinsulin. Genetics 196: 557–567. https://doi.org/10.1534/genetics.113.157800

Huang W., A. Massouras, Y. Inoue, J. Peiffer, M. Ràmia, *et al.*, 2014 Natural variation in genome architecture among 205 Drosophila melanogaster Genetic Reference Panel lines. Genome Res. 24: 1193–208. https://doi.org/10.1101/gr.171546.113

Jin S., S. Martinek, W. S. Joo, J. R. Wortman, N. Mirkovic, *et al.*, 2000 *Identification and characterization of a p53 homologue in Drosophila melanogaster*. National Academy of Sciences.

Johnson S., S. Halford, A. G. Morris, R. J. Patel, S. E. Wilkie, *et al.*, 2003 Genomic organisation and alternative splicing of human RIM1, a gene implicated in autosomal dominant cone-rod dystrophy (CORD7). Genomics 81: 304–314. https://doi.org/10.1016/S0888-7543(03)00010-7

Kanda H., and M. Miura, 2004 Regulatory Roles of JNK in Programmed Cell Death. J. Biochem. 136: 1–6. https://doi.org/10.1093/jb/mvh098

Kang M. J., J. Chung, and H. D. Ryoo, 2012 CDK5 and MEKK1 mediate pro-apoptotic signalling following endoplasmic reticulum stress in an autosomal dominant retinitis pigmentosa model. Nat. Cell Biol. 14: 409–415. https://doi.org/10.1038/ncb2447

Koken M. H. M., C. Vreeken, S. A. M. Bol, N. C. Cheng, I. Jaspers-Dekker, *et al.*, 1992 Cloning and characterization of the *Drosophila* homolog of the xeroderma pigmentosum complementation-group B correcting gene, *ERCC3*. Nucleic Acids Res. 20: 5541–5548. https://doi.org/10.1093/nar/20.21.5541

Kraemer K. H., and J. J. DiGiovanna, 2016 Xeroderma Pigmentosum

Kurtishi A., B. Rosen, K. S. Patil, G. W. Alves, and S. G. Møller, 2018 Cellular Proteostasis in Neurodegeneration. Mol. Neurobiol. https://doi.org/10.1007/s12035-018-1334-z

Laflamme C., G. Assaker, D. Ramel, J. F. Dorn, D. She, *et al.*, 2012 Evi5 promotes collective cell migration through its Rab-GAP activity. J. Cell Biol. 198: 57–67. https://doi.org/10.1083/jcb.201112114

Lavoy S., V. G. Chittoor-Vinod, C. Y. Chow, and I. Martin, 2018 Genetic Modifiers of Neurodegeneration in a Drosophila Model of Parkinson's Disease. Genetics 209: 1345–1356. https://doi.org/10.1534/genetics.118.301119

Lu Q., K. Ding, M. P. Frosch, S. Jones, M. Wolfe, *et al.*, 2010 Alzheimer's disease-linked presenilin mutation (PS1M146L) induces filamin expression and γ-secretase independent redistribution. J. Alzheimers. Dis. 22: 235–45. https://doi.org/10.3233/JAD-2010-100585

Mackay T. F. C., S. Richards, E. A. Stone, A. Barbadilla, J. F. Ayroles, *et al.*, 2012 The Drosophila melanogaster Genetic Reference Panel. Nature 482: 173–178. https://doi.org/10.1038/nature10811

Mattson M. P., 2000 Apoptosis in neurodegenerative disorders. Nat. Rev. Mol. Cell Biol. 1: 120–130. https://doi.org/10.1038/35040009

McLaughlin H. M., R. Sakaguchi, C. Liu, T. Igarashi, D. Pehlivan, *et al.*, 2010 Compound Heterozygosity for Loss-of-Function Lysyl-tRNA Synthetase Mutations in a Patient with Peripheral Neuropathy. Am. J. Hum. Genet. 87: 560–566. https://doi.org/10.1016/J.AJHG.2010.09.008

Minárik P., N. Tomášková, M. Kollárová, and M. Antalík, 2002 *Malate Dehydrogenases-Structure and Function*.

Mollereau B., and D. Ma, 2014 The p53 control of apoptosis and proliferation: lessons from Drosophila. Apoptosis 19: 1421–9. https://doi.org/10.1007/s10495-014-1035-7

Montojo J., K. Zuberi, H. Rodriguez, F. Kazi, G. Wright, *et al.*, 2010 GeneMANIA Cytoscape plugin: fast gene function predictions on the desktop. Bioinformatics 26: 2927–8. https://doi.org/10.1093/bioinformatics/btq562

Mounkes L. C., R. S. Jones, B.-C. Liang, W. Gelbart, and M. T. Fuller, 1992 A Drosophila model for xeroderma pigmentosum and Cockayne's syndrome: haywire encodes the fly homolog of ERCC3, a human excision repair gene. Cell 71: 925–937. https://doi.org/10.1016/0092-8674(92)90389-T

Mulligan K. A., C. Fuerer, W. Ching, M. Fish, K. Willert, *et al.*, 2012 Secreted Wingless-interacting molecule (Swim) promotes long-range signaling by maintaining Wingless solubility. Proc. Natl. Acad. Sci. U. S. A. 109: 370–7. https://doi.org/10.1073/pnas.1119197109

Nadeau J. H., 2001 Modifier genes in mice and humans. Nat Rev Genet 2: 165–174. https://doi.org/10.1038/35056009

Ouyang L., Z. Shi, S. Zhao, F.-T. Wang, T.-T. Zhou, *et al.*, 2012 Programmed cell death pathways in cancer: a review of apoptosis, autophagy and programmed necrosis. Cell Prolif. 45: 487–498. https://doi.org/10.1111/j.1365-2184.2012.00845.x

Pećina-Slaus N., 2010 Wnt signal transduction pathway and apoptosis: a review. Cancer Cell Int. 10: 22. https://doi.org/10.1186/1475-2867-10-22

Pollard P. J., J. J. Brière, N. A. Alam, J. Barwell, E. Barclay, *et al.*, 2005 Accumulation of Krebs cycle intermediates and over-expression of HIF1α in tumours which result

690 from germline FH and SDH mutations. Hum. Mol. Genet. 14: 2231–2239.
691 https://doi.org/10.1093/hmg/ddi227

692 Queitsch C., K. D. Carlson, and S. Girirajan, 2012 Lessons from model organisms:
693 phenotypic robustness and missing heritability in complex disease. PLoS Genet 8:
694 e1003041. https://doi.org/10.1371/journal.pgen.1003041

695 Rasmussen M., N. Ortolano, A. Romero-Morales, V. Gama, M. L. Rasmussen, *et al.*,
696 2018 Wnt Signaling and Its Impact on Mitochondrial and Cell Cycle Dynamics in
697 Pluripotent Stem Cells. Genes (Basel). 9: 109.
698 https://doi.org/10.3390/genes9020109

699 Reynaud E., H. Lomelí, M. Vázquez, and M. Zurita, 1999 The *Drosophila melanogaster*
700 Homologue of the Xeroderma Pigmentosum D Gene Product Is Located in
701 Euchromatic Regions and Has a Dynamic Response to UV Light-induced Lesions
702 in Polytene Chromosomes, (E. H. Blackburn, Ed.). Mol. Biol. Cell 10: 1191–1203.
703 https://doi.org/10.1091/mbc.10.4.1191

704 Rives A. F., K. M. Rochlin, M. Wehrli, S. L. Schwartz, and S. DiNardo, 2006 Endocytic
705 trafficking of Wingless and its receptors, Arrow and DFrizzled-2, in the Drosophila
706 wing. Dev. Biol. 293: 268–283. https://doi.org/10.1016/J.YDBIO.2006.02.006

707 Sandu C., H. D. Ryoo, and H. Steller, 2010 Drosophila IAP antagonists form multimeric
708 complexes to promote cell death. J. Cell Biol. 190: 1039–52.
709 https://doi.org/10.1083/jcb.201004086

710 Sano R., and J. C. Reed, 2013 ER stress-induced cell death mechanisms. Biochim
711 Biophys Acta 1833: 3460–3470. https://doi.org/10.1016/j.bbamcr.2013.06.028

712 Scriver C. R., and P. J. Waters, 1999 Monogenic traits are not simple: lessons from
713 phenylketonuria. Trends Genet 15: 267–272.

714 Sellar G. C., K. P. Watt, G. J. Rabiasz, E. A. Stronach, L. Li, *et al.*, 2003 OPCML at
715 11q25 is epigenetically inactivated and has tumor-suppressor function in epithelial
716 ovarian cancer. Nat. Genet. 34: 337–343. https://doi.org/10.1038/ng1183

717 Shannon P., A. Markiel, O. Ozier, N. S. Baliga, J. T. Wang, *et al.*, 2003 Cytoscape: a
718 software environment for integrated models of biomolecular interaction networks.
719 Genome Res. 13: 2498–504. https://doi.org/10.1101/gr.1239303

720 Shiratsuchi T., H. Nishimori, H. Ichise, Y. Nakamura, and T. Tokino, 1997 Cloning and
721 characterization of BAI2 and BAI3, novel genes homologous to brain-specific
722 angiogenesis inhibitor 1 (BAM). Cytogenet. Genome Res. 79: 103–108.
723 https://doi.org/10.1159/000134693

724 Shiratsuchi T., K. Oda, H. Nishimori, M. Suzuki, E. Takahashi, *et al.*, 1998 Cloning and
725 Characterization of BAP3 (BAI-Associated Protein 3), a C2 Domain-Containing
726 Protein That Interacts with BAI1. Biochem. Biophys. Res. Commun. 251: 158–165.
727 https://doi.org/10.1006/BBRC.1998.9408

728 Shklover J., F. Levy-Adam, and E. Kurant, 2015 The role of Drosophila TNF Eiger in
729 developmental and damage-induced neuronal apoptosis. FEBS Lett. 589: 871–879.
730 https://doi.org/10.1016/j.febslet.2015.02.032

731 Shlevkov E., and G. Morata, 2012 A dp53/JNK-dependant feedback amplification loop
732 is essential for the apoptotic response to stress in Drosophila. Cell Death Differ. 19:
733 451–460. https://doi.org/10.1038/cdd.2011.113

734 Subramanian A., P. Tamayo, V. K. Mootha, S. Mukherjee, B. L. Ebert, *et al.*, 2005 Gene
735 set enrichment analysis: a knowledge-based approach for interpreting genome-
736 wide expression profiles. Proc. Natl. Acad. Sci. U. S. A. 102: 15545–50.
737 https://doi.org/10.1073/pnas.0506580102

738 The Multiple Leiomyoma Consortium, 2002 Germline mutations in FH predispose to
739 dominantly inherited uterine fibroids, skin leiomyomata and papillary renal cell
740 cancer. Nat. Genet. 30: 406–410. https://doi.org/10.1038/ng849

741 Waters M. F., N. A. Minassian, G. Stevanin, K. P. Figueroa, J. P. A. Bannister, *et al.*,
742 2006 Mutations in voltage-gated potassium channel KCNC3 cause degenerative
743 and developmental central nervous system phenotypes. Nat. Genet. 38: 447–451.
744 https://doi.org/10.1038/ng1758

745 Wolff T., and D. F. Ready, 1991 Cell death in normal and rough eye mutants of
746 Drosophila. Development 113: 825–839. https://doi.org/8223268

747 Zhou X., and M. Stephens, 2012 Genome-wide efficient mixed-model analysis for
748 association studies. Nat. Genet. 44: 821–4. https://doi.org/10.1038/ng.2310

749

750 **FIGURE LEGENDS**

751 **Figure 1. Activation of apoptosis through *p53* and *rpr*-associated pathways.**

752 Apoptosis is primarily initiated through either p53 or Jun-induced (JNK) transcriptional
753 activation of the Inhibitor of Apoptosis (IAP, in *Drosophila* Diap) inhibitors *hid*, *rpr* and
754 *grim*. While p53 is primarily activated by DNA damage and disruption of the cell cycle,
755 JNK signaling is activated downstream of cellular stress, such as endoplasmic reticulum
756 (ER) stress, through Ire1 and Cdk5. ER stress occurs when misfolding proteins, like the
757 rhodopsin mutant $Rh1^{G69D}$, accumulate in the ER (Chow *et al.* 2016). Expression of *rpr*,
758 *grim*, and *hid* leads to inhibition of Diap1, releasing the inhibition on initiator caspases

and allows for the activation of effector caspases and downstream apoptosis. Models used in this or previous studies of retinal degeneration in the DGRP are indicated in white.

Figure 2. Apoptosis levels vary across genetic background in *p53* and *rpr* models of apoptosis-induced degeneration.

Apoptosis induced by overexpression of *p53* (**A**) or *rpr* (**B**), as measured by adult eye size, varies across different genetic backgrounds. DGRP strains are arranged along the X-axis from smallest to largest (median eye size ± standard deviation). Representative images of *GMR>p53* eyes (**C**) or *GMR-rpr* eyes (**D**) in different DGRP backgrounds demonstrate the phenotypic variation quantified in panels **A** and **B**.

Figure 3. Eye size is correlated between *GMR-rpr* and both *GMR>p53* and *GMR>Rh1^{G69D}* models of degeneration.

Correlation in mean eye size between the *GMR-rpr*, *GMR>p53*, and *GMR>Rh1^{G69D}* models across the DGRP. **A.** Eye size is significantly correlated in the same DGRP strains expressing *GMR-rpr* and *GMR>p53* ($r = 0.19$, $P = 0.0071$). **B.** Eye size is significantly correlated in the same DGRP strains expressing *GMR-rpr* and *GMR>Rh1^{G69D}* ($r = 0.25$, $P = 0.001$). **C.** Eye size is not correlated in same DGRP strains expressing *GMR>p53* and *GMR>Rh1^{G69D}* ($r = 0.12$, $P = 0.13$). * $P < 0.05$, ** $P < 0.005$.

Figure 4. *rpr* modifiers are enriched for neuronal function, Wnt signaling, and metabolic pathways.

A. *rpr* modifier network, as plotted by the GeneMANIA plugin in Cytoscape (Shannon *et al.* 2003; Montojo *et al.* 2010). Significant candidate modifiers are indicated in red, with physical interactions shown in green, genetic interactions shown in blue, and predicted interactions shown in gray. Circles represent groups with a functional identifier. **B.** Top 20 significant ontological categories as identified by GSEA. Categories are arranged from most significant on top to least significant along the y-axis. P-values are indicated by red-to-blue gradient, with red the lowest p-values and blue the highest P-values. Gene number identified in each category is indicated along the y-axis.

Figure 5. Knockdown of candidate *rpr* modifiers significantly alters apoptosis-induced degeneration.

RNAi against candidate modifiers was expressed under the control of *GMR-GAL4* in the *GMR-rpr* model. The genetically matched attP2 line was crossed into the *GMR-rpr* line as a control (blue). Eye size in pixels was quantified for N = 11-15 flies per strain and plotted with the 25^{th}-75^{th} percentile of measurements in the central box. Measurements lying outside of 1.5 x interquartile range are indicated as points. Representative images of each line are found above the data for that line. Knockdown of *LIMK1* or *swim* significantly reduces eye size in the *GMR-rpr* model of degeneration compared to controls. Loss of *Sema1a*, *MED16*, or *hay* results in a significant increase in eye size compared to controls. Loss of *CG1907* does not significantly alter eye size, but changes in pigmentation are similar in the presence or absence of GMR-rpr (SUPP FIG). Loss of *αManA1*, *LysRS*, or *CG3032* do not produce a significant effect. RNAi lines with

804 significant changes in eye size are indicated in red, while those that are not significantly

805 changed are indicated in white. * $P < 0.05$, *** $P < 0.0005$.

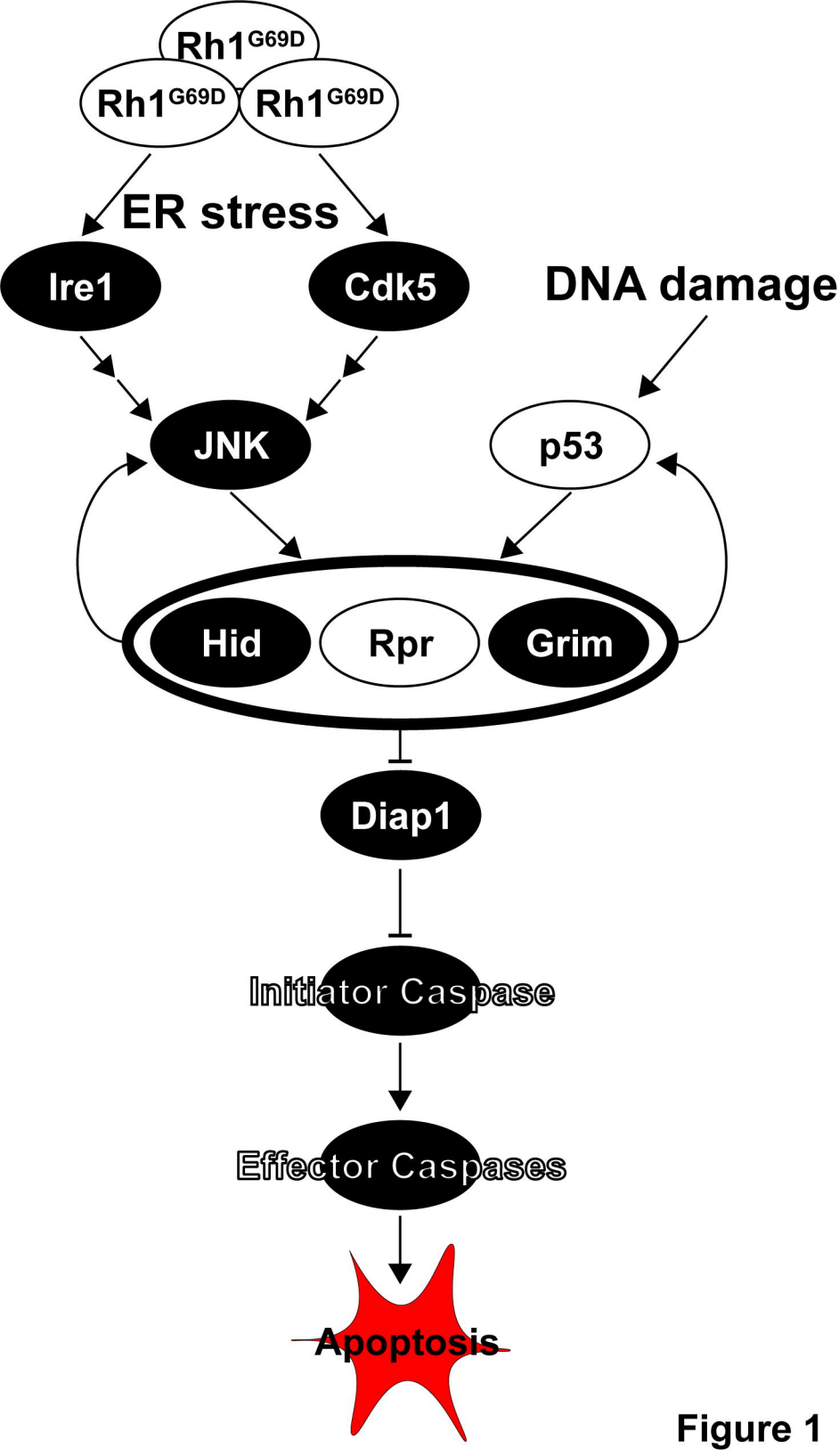
Rh1G69D
Rh1G69D
Rh1G69D
ER stress
Ire1
Cdk5
DNA damage
JNK
p53
Hid
Rpr
Grim
Diap1
Initiator Caspase
Effector Caspases
Apoptosis

Figure 1

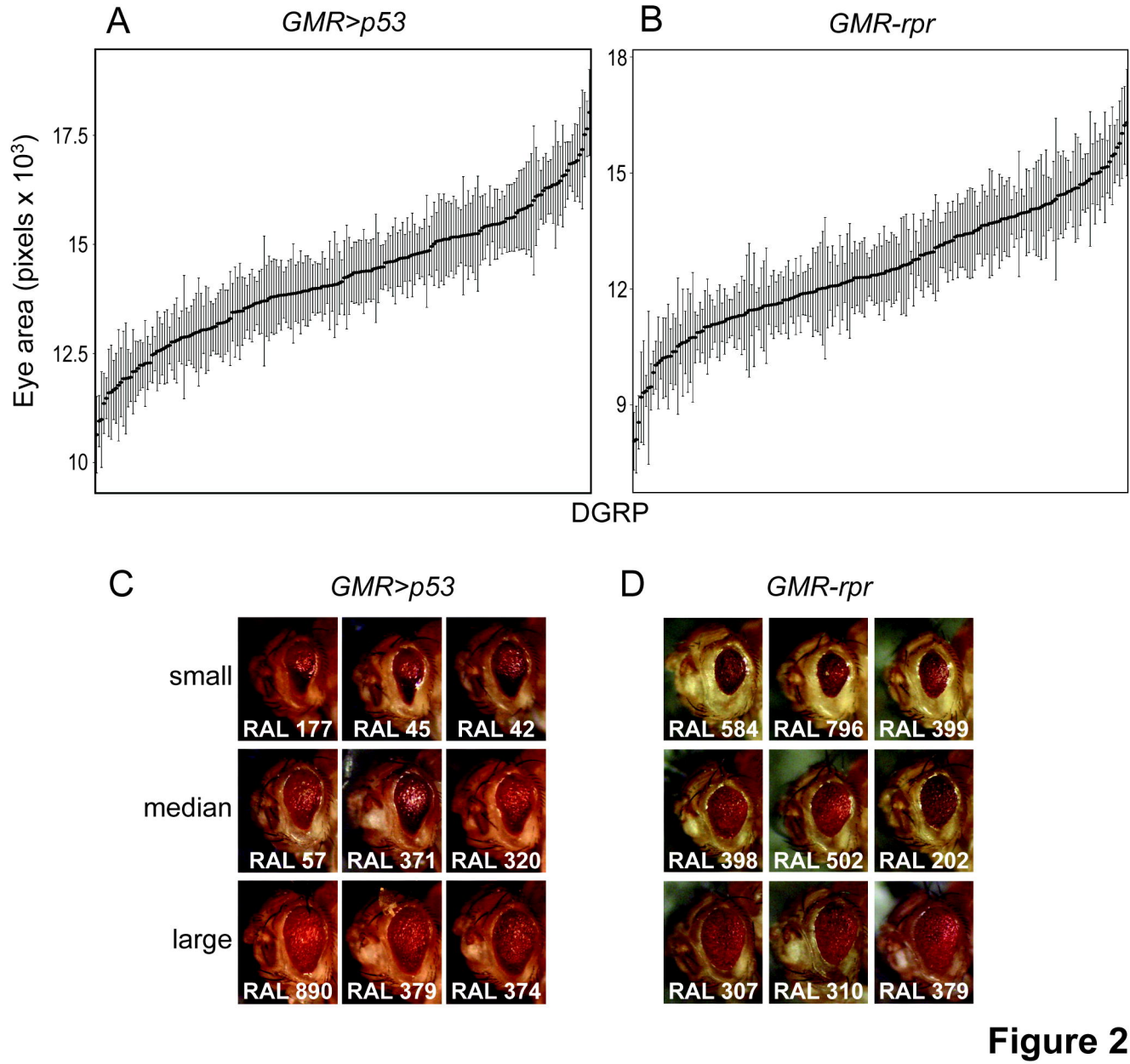
A
GMR>p53
B
GMR-rpr
Eye area (pixels x 10^3)
17.5
15
12.5
10
18
15
12
9
DGRP
C
GMR>p53
D
GMR-rpr
small
median
large
RAL 177
RAL 45
RAL 42
RAL 57
RAL 371
RAL 320
RAL 890
RAL 379
RAL 374
RAL 584
RAL 796
RAL 399
RAL 398
RAL 502
RAL 202
RAL 307
RAL 310
RAL 379

Figure 2

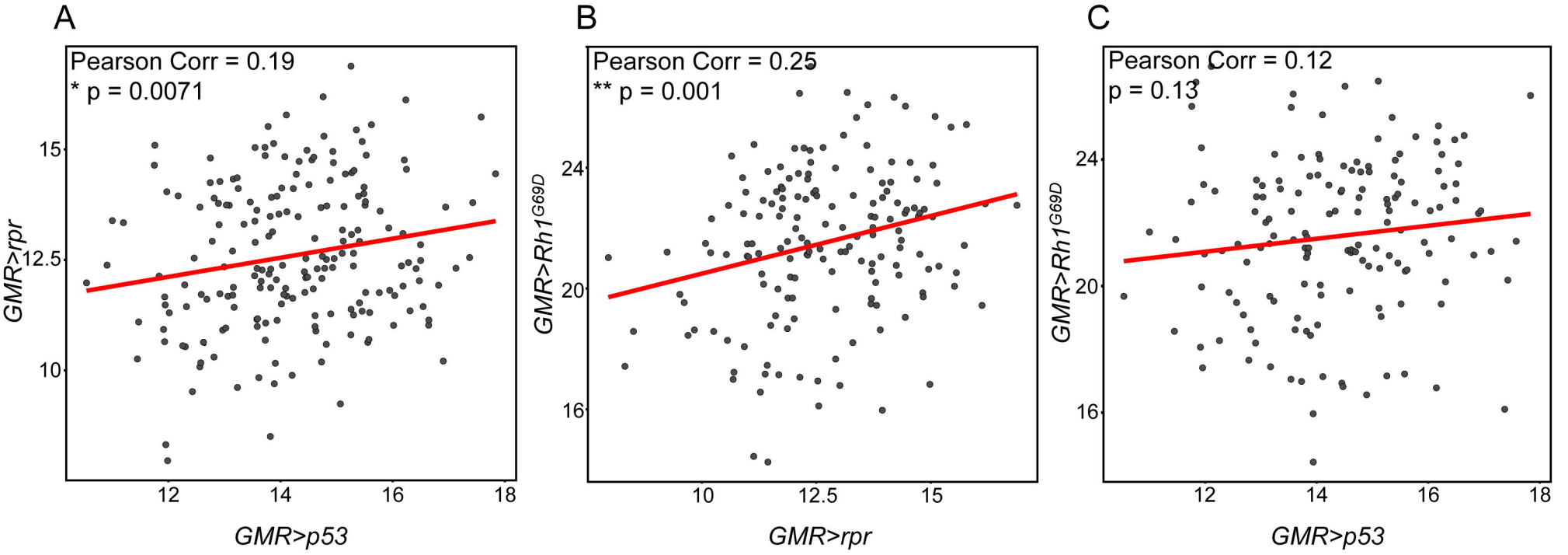
A
Pearson Corr = 0.19
* p = 0.0071
GMR>rpr
GMR>p53
B
Pearson Corr = 0.25
** p = 0.001
GMR>Rh1G69D
GMR>rpr
C
Pearson Corr = 0.12
p = 0.13
GMR>Rh1G69D
GMR>p53

Figure 3

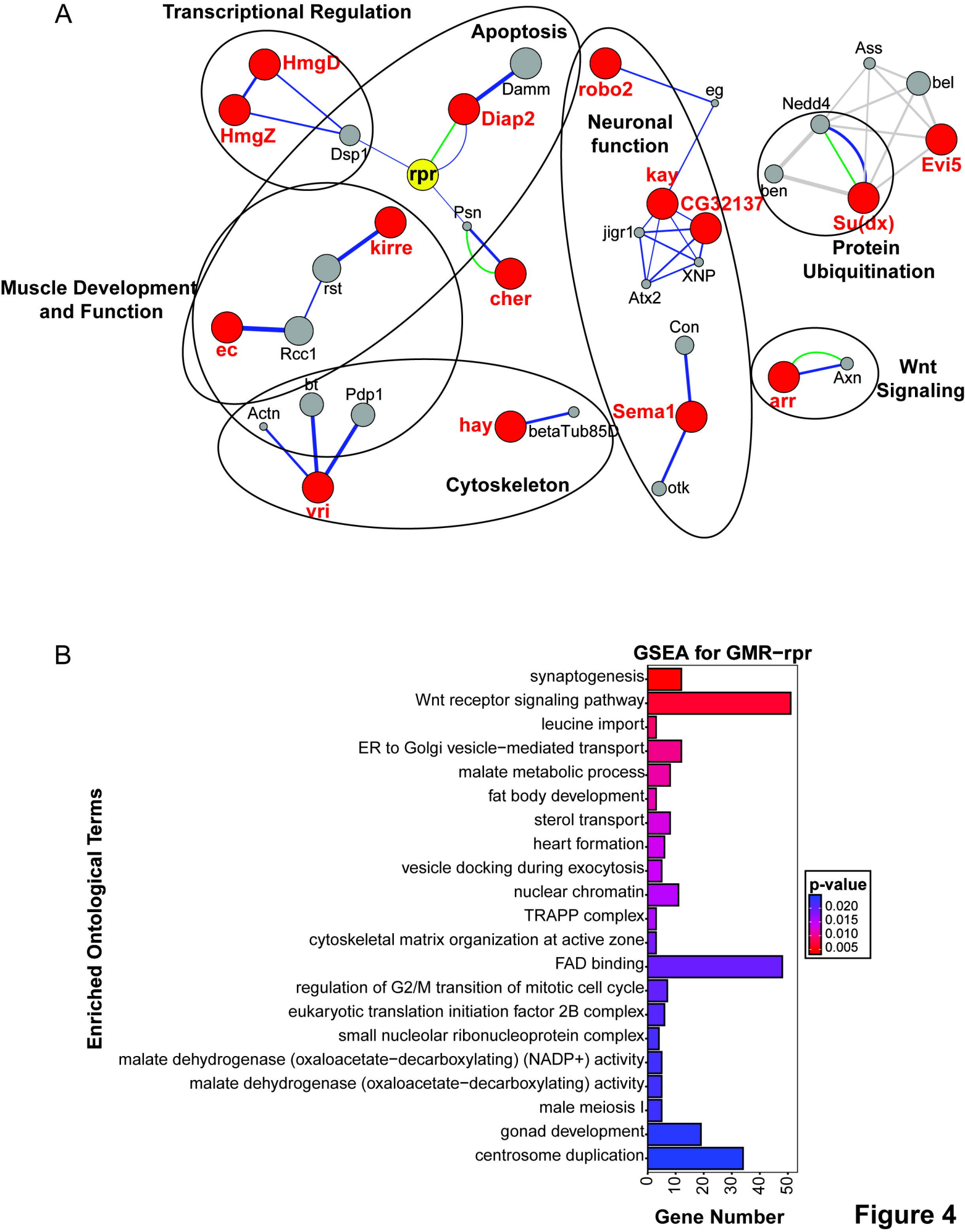
A
Transcriptional Regulation
Apoptosis
Neuronal function
Protein Ubiquitination
Muscle Development and Function
Wnt Signaling
Cytoskeleton
HmgD
HmgZ
Dsp1
Damm
Diap2
rpr
Psn
cher
robo2
eg
kay
CG32137
jigr1
XNP
Atx2
Ass
bel
Nedd4
Evi5
ben
Su(dx)
kirre
rst
ec
Rcc1
Con
Axn
arr
Sema1
otk
bt
Pdp1
Actn
hay
betaTub85D
vri
B
GSEA for GMR−rpr
synaptogenesis
Wnt receptor signaling pathway
leucine import
ER to Golgi vesicle−mediated transport
malate metabolic process
fat body development
sterol transport
heart formation
vesicle docking during exocytosis
nuclear chromatin
TRAPP complex
cytoskeletal matrix organization at active zone
FAD binding
regulation of G2/M transition of mitotic cell cycle
eukaryotic translation initiation factor 2B complex
small nucleolar ribonucleoprotein complex
malate dehydrogenase (oxaloacetate−decarboxylating) (NADP+) activity
malate dehydrogenase (oxaloacetate−decarboxylating) activity
male meiosis I
gonad development
centrosome duplication
Enriched Ontological Terms
p-value
0.020
0.015
0.010
0.005
0
10
20
30
40
50
Gene Number

Figure 4

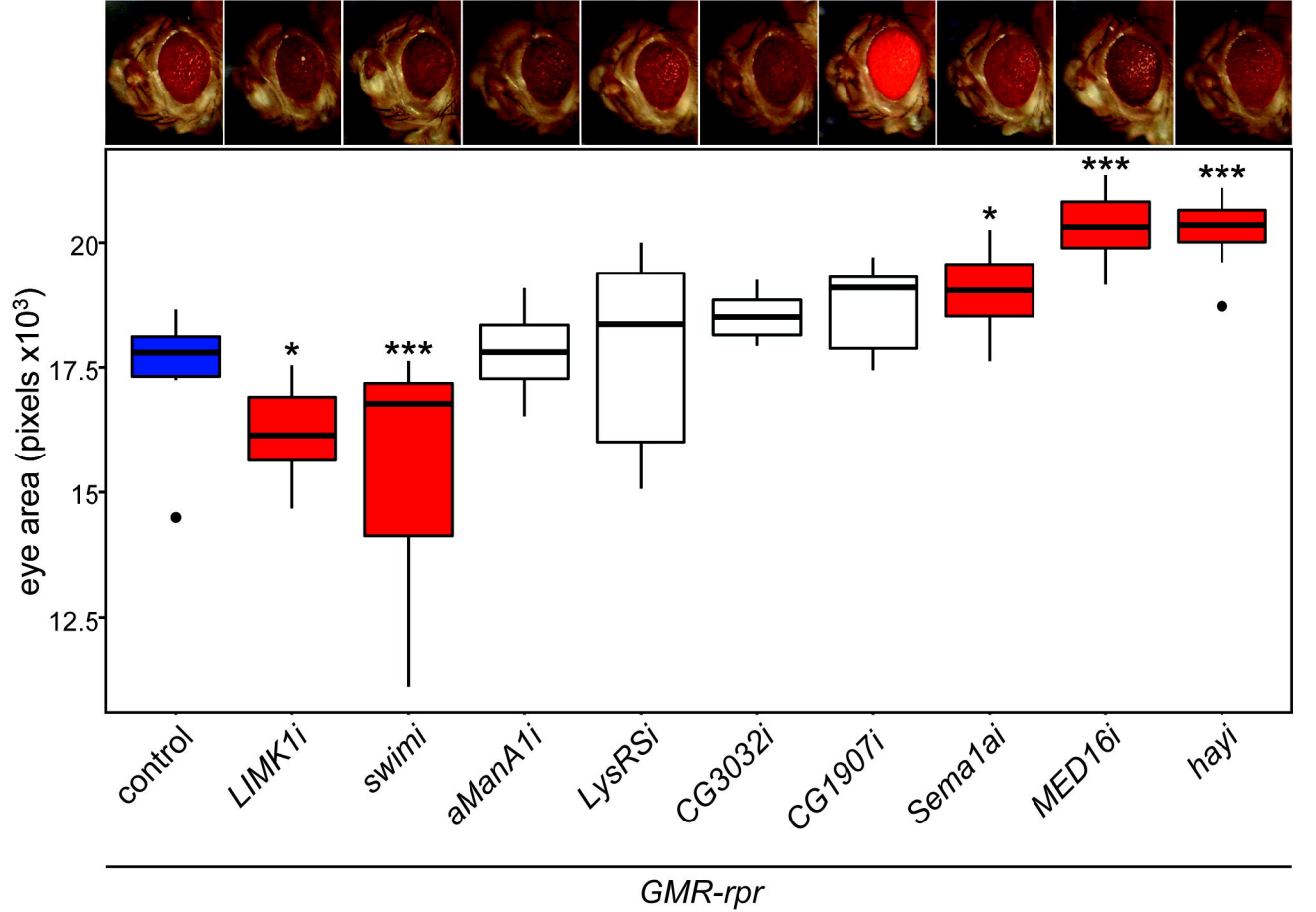
eye area (pixels x10^3)
20
17.5
15
12.5
*
***
*
***
***
control
LIMK1i
swimi
aManA1i
LysRSi
CG3032i
CG1907i
Sema1ai
MED16i
hayi
GMR-rpr

Figure 5